

Exactly Defined Half-Stemmed Polymer Lamellar Crystals with Precisely Controlled Defects' Locations

Xue-Hui Dong,[†] Ryan Van Horn,^{†,‡} Ziran Chen,[†] Bo Ni,[†] Xinfei Yu,[†] Andreas Wurm,[‡] Christoph Schick,[‡] Bernard Lotz,[§] Wen-Bin Zhang,^{*,†} and Stephen Z. D. Cheng^{*,†}

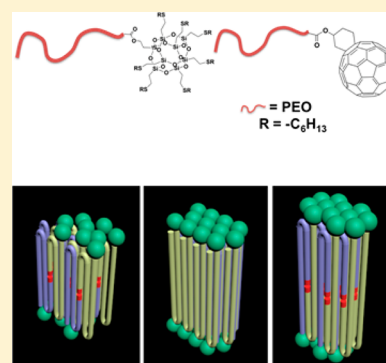
[†]Department of Polymer Science, College of Polymer Science and Polymer Engineering, The University of Akron, Akron, Ohio 44325-3909, United States

[‡]Institute of Physics, University of Rostock, Wismarsche Strasse 43-45, 18051 Rostock, Germany

[§]Institut Charles Sadron (CNRS-Université de Strasbourg), 23 Rue du Loess, F-67034 Strasbourg, France

S Supporting Information

ABSTRACT: We describe highly unconventional situations in which the polymer chain ends remain trapped in and are located in the middle of the lamellar crystal core as defects. Such structures are observed in giant molecular shape amphiphiles constructed by a polyhedral silsesquioxane (POSS) nanoparticle tethered with a poly(ethylene oxide) (PEO) tail. The cross-sectional area of the POSS located on the PEO lamellar surfaces imposes that the crystalline, chain-folded PEO tails generate a surface area that is at least comparable to the POSS requirements. Metastable PEO crystal structures with 1.5, 2, and 2.5 stem numbers have been observed with different thermodynamic stabilities.



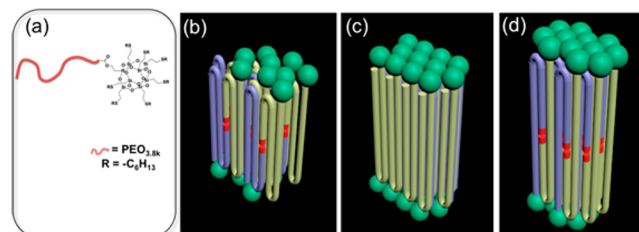
SECTION: Glasses, Colloids, Polymers, and Soft Matter

Observation of lamellar crystals with integral folding (IF) in low molecular weight (LMW) poly(ethylene oxide) fractions (PEO) has been one of the major progresses in the understanding of polymer crystallization started more than half of a century ago.^{1–5} Similar observations were found for long *n*-alkanes (up to C₃₀₀) with uniform chain lengths.⁶ The formation of these IFs in LMW polymers indicates that the crystal is more stable when all of the chain ends are rejected to the folded/end surfaces.^{2–6} The IF crystals are denoted as the crystals with extended (containing one stem for each chain, with folding number *n* = 0 and stem number *s* = 1), once-folded (two stems per chain, *n* = 1 and *s* = 2), twice-folded chains (three stems per chain, *n* = 2, and *s* = 3), and so forth.

In situ, time-resolved synchrotron small-angle X-ray scattering (SAXS) results first on *n*-alkanes^{7–10} and then on LMW PEO fractions^{11–15} have shown that in melt crystallization, the chains do not immediately reach the IF states. Rather, they first form nonintegral folded (NIF) crystals,^{7–15} which are thermodynamically less stable but formed more rapidly. The initial NIF crystals transfer to IF crystals via annealing processes.^{7–18} These processes drive chain ends, which are probably coupled in pairs and initially randomly distributed in the lamellar core, toward the lamellar surface, and it is a universal trend in polymer crystallization.¹⁸ It is most clearly observed for LMW PEO and *n*-alkanes and persists up to MWs for which the changes in lamellar thickness for *s* and *s* + 1 stems are no longer detectable.¹⁴

On the other hand, exactly defined half-stemmed crystals with the stem numbers of 1.5, 2.5, and so forth using LMW PEO fractions as an example must contain end pairs located at the center to form a sheet parallel to the lamellar surface containing discrete end pair defects within the crystals (Scheme 1). This structure is in sharp contrast with a well-established rule of polymer crystallization stating that the chain ends are preferably rejected at the lamellar surfaces. In normal LMW PEO crystallization, this type of crystal cannot be isolated and observed because within the NIF lamellar crystals initially

Scheme 1. Schematic Drawing of the Molecular Structure (a) and IF and Half-Stemmed Crystals of GMSAs with *s* = 2.5 (b), *s* = 2.0 (c), and *s* = 1.5 (d)



Received: June 1, 2013

Accepted: July 1, 2013

Published: July 1, 2013

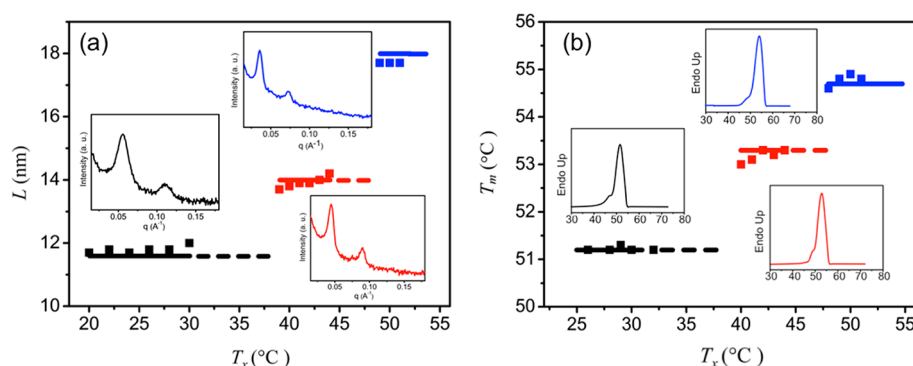


Figure 1. Relationships between the L and T_x (a) and the T_m and T_x (b) for HPOSS-PEO_{3.8k}. Solid squares represent experimental data of the PEO($s = 2.5$) (black), PEO($s = 2$) (red), and PEO($s = 1.5$) (blue) crystals. Solid and dashed lines are the calculated values (see text).

formed, the chain end pairs are randomly located, and they are continuously driven toward the crystal surfaces to form IF crystals.^{7–18} The exactly defined half-stemmed crystals do not thus possess a local free-energy minimum (a metastable state) in the normal LMW PEO crystallization. The question now is can we specifically design chain molecules to create a local free-energy minimum and make this type of exactly defined half-stemmed crystals become stable enough and experimentally observable?

The molecular design in this study was to connect a LMW PEO chain as a tail with one nanoparticle (NP), hexyl-substituted polyhedral silsesquioxane (HPOSS), to become a new class of materials, giant molecular shape amphiphiles (GMSAs).^{19–21} The molecular architecture is shown in Scheme 1. When PEO is crystallized, the POSS moieties are located at the PEO lamellar crystals' surfaces. In order to balance the cross-sectional areas of HPOSS and PEO stems, the latter may adopt a highly unusual structure with exactly defined half stems and chain end pairs located at the center of the PEO lamellar crystals. Apparently, the GMSAs are similar to diblock copolymers with one block being crystallizable.^{22–31} However, in our case, noncrystalline HPOSS possesses fixed shape and volume, thus with a constant cross-sectional area. When the PEO tails crystallize, HPOSS groups are rejected onto the crystal fold/end surface, and the surface area generated by the number of PEO stems from two PEO tails must be larger or comparable with the cross-sectional area of each HPOSS (Scheme 1). Synthesis of HPOSS-PEO is described in the Supporting Information (SI) (Figures S1 and S2). The cross-sectional area of HPOSS is estimated to be 0.65 (with no substituent groups) to 0.833 nm² (with the isobutyl substituent groups).³² The cross-sectional area of each PEO stem in the monoclinic unit cell is 0.214 nm².^{2–5} To first approximation, the cross-sectional area of one HPOSS requires at least three PEO stems in the lattice to reach close packing with its squeezed neighboring HPOSSs on the PEO lamellar fold/end surfaces.

In this study, we use a PEO fraction with a MW of 3.8k g/mol because this fraction can usually form either PEO($s = 2$) crystals with a stem length of 12.0 nm or PEO($s = 1$) crystals with a stem length of 24.0 nm, depending on supercooling (crystallization temperature, T_x) (see Figure S3 in the SI).^{2–5,12–14} Figure 1a shows a plot of the long periods (L) measured by SAXS experiments and T_x for HPOSS-PEO_{3.8k}. Three invariant L regions exist, $L = 11.8$ nm when $T_x < 30$ °C, $L = 14.0$ nm when 40 °C $< T_x < 45$ °C, and $L = 17.8$ nm above $T_x = 49$ °C (within a deviation of ± 0.2 nm). All of the SAXS

patterns display sharp first-order peaks together with their second-order peaks (the insets of Figure 1a), indicating long range ordered lamellar crystals. However, the third-order peaks are not observed due probably to the asymmetric volume fractions of HPOSS and PEO. In the case within $40 < T_x < 45$ °C, the $L = 14.0$ nm must correspond to the PEO($s = 2$) crystals ($24.0/2 + 1.0 \times 2 = 14.0$ nm; the dimension along the lamellar normal direction for one HPOSS with its linker to PEO tail is ~ 1.0 nm). The two PEO tails in the PEO($s = 2$) crystals give rise to four PEO stems with an area of 0.856 nm², and two HPOSS NPs are located at the opposite crystal surfaces with an occupied area of 0.833 nm² for each POSS.

However, the observed L values of 11.8 and 17.7 nm do not fit with either the PEO($s = 1$) or PEO($s = 3$) crystals. In order to match these two periodicities in a consistent way, one must assume that some of the PEO stems span only half of the PEO lamellar thickness. On the basis of this assumption, the two periodicities can be neatly accounted for PEO($s = 2.5$) ($24.0/2.5 + 1.0 \times 2 = 11.6$ nm) and PEO($s = 1.5$) ($24.0/1.5 + 1.0 \times 2 = 18.0$ nm). The surface areas that are available for the HPOSS moieties are thus 1.070 and 0.642 nm², respectively. Whereas the 2.5 stems per PEO tail situation leaves ample room for the HPOSS, the 1.5 one suggests that the HPOSS groups are somewhat squeezed at the lamellar surface due to the fact that the decrease of free energy caused by PEO crystallization overwrites that originated by the squeezed HPOSS groups (see below). Furthermore, it is also clear that these constraints are not compatible with a complete extended PEO tail, as is the case for the homopolymer. Due to the HPOSS encumbrance on the fold surface, the 1.5 stems version becomes the highest possible extension of the PEO tails.

The remaining issue is the L values in two T_x regions represented by the dashed lines in Figure 1. Within $30 < T_x < 39$ °C, for example, the initial L of the PEO crystallization was observed to be 11.8 nm; however, L continuously increased with crystallization time, recognized as a thickening process. The L could ultimately approach 14 nm to become the PEO($s = 2$) crystals. Similar observations can also be made in the T_x region of $45 < T_x < 49$ °C. The initial L is located at 14 nm and then approaches 17.8 nm when the time is further prolonged via the thickening process, implying sufficient molecular mobility within the crystals (see Figure S4 in the SI).

In order to understand the thermodynamic stabilities of these crystals, the relationship between the melting temperature (T_m) and T_x for HPOSS-PEO_{3.8k} is shown in Figure 1b. This relationship resembles that between the L and T_x as shown in Figure 1a. Three constant T_m s are observed. For the PEO($s =$

2.5) and PEO($s = 2$) crystals, because the thickening process becomes extremely fast during heating, we utilized ultrafast chip differential scanning calorimetry (DSC)³³ at a heating rate of 100 000 K/sec to ensure that their T_m values are not changed during heating caused by the changes of their metastabilities.¹⁸ For these PEO($s = 2.5$), PEO($s = 2$), and PEO($s = 1.5$) crystals, their T_m values correspond to 51.3, 53.3, and 54.5 °C, respectively (with a deviation of ± 0.3 °C). The PEO crystallinities of HPOSS-PEO_{3.8k} detected in the DSC experiments are very close to those in pure LMW PEO fractions (>92%) (evidence to illustrate that all of the PEO tails are crystallized).

The constraints set by the POSS nanoparticle at the PEO lamellar surfaces were put to a further test by replacing the noncrystallizable HPOSS heads with an isobutyl-POSS head (BPOSS) that can crystallize (synthesis and characterization of this new GMSA are discussed in SI Figures S1 and S2). Care was taken to maintain the same PEO tail lengths. In order to avoid the disturbance of the BPOSS crystallization that takes place dominantly at a higher temperature on the PEO tail crystallization in the melt, single crystals were produced in a 1:1 mixture of amyl acetate and octane that was used to produce PEO single crystals, as reported in the past.^{34–36} Depending on T_c , BPOSS-PEO single crystals with $s = 2.5$ or 2 are obtained, as attested by their lamellar thickness measured by AFM (insets in Figure 2). 1D wide-angle X-ray diffraction (WAXD) patterns of

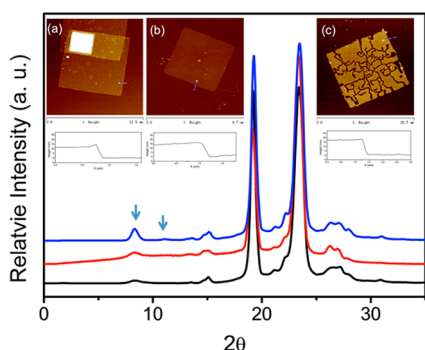


Figure 2. Set of 1D WAXD patterns for BPOSS-PEO_{3.8k} single-crystal mats with PEO($s = 2.5$) (black), PEO($s = 2.0$) (red) crystals from solution crystallization, and PEO($s = 1.5$) (blue) by annealing the PEO($s = 2.5$) crystal at 52 °C. AFM single-crystal morphologies of PEO($s = 2.5$) (a), PEO($s = 2.0$) (b), and PEO($s = 1.5$) (c) crystals are also shown in the insets.

single-crystal mats indicate that the BPOSSs are not crystallized. In the expected 2θ range ($\sim 8^\circ$) only an amorphous halo is present (black and red curves in Figure 2). Annealing the PEO($s = 2.5$) at 52 °C induces a lamellar thickening from $s = 2.5$ to 1.5 (cf. the two AFM profiles insets in Figure 2a and c). Also, the thickening process induces significant cracks (Figure 2c) in the initially smooth crystals (Figure 2a). Furthermore, the WAXD patterns show additional peaks at 8.3 and 11.1°, indicating that as a result of the annealing, the BPOSS layers have reached a crystalline order, and therefore, some form of close packing is achieved on the fold/end PEO lamellar surface. Again, the crystallinity of PEO is >92%. In addition, disregarding whether the BPOSS groups are in the ordered or disordered layers, their surfaces are smooth, as observed in the AFM experiments, indicating that these BPOSS groups are located within a single layer on the top of the crystal surface. More telling are the differences in the T_m values. For the PEO(s

$= 1.5$) crystals with the “crystalline” BPOSS layers, its T_m is 4.7 °C higher than that of the corresponding HPOSS-PEO($s = 1.5$), in which the HPOSS layer is amorphous.

Comparing these T_m values in Figure 1b for HPOSS-PEO_{3.8k}, the difference of T_m s between PEO($s = 2.5$) and PEO($s = 2$) crystals is larger than that between PEO($s = 2$) and PEO($s = 1.5$) crystals. These differences are analytically associated with four parameters, the lamellar thicknesses and thus fold/end surface free energy, $\gamma_e(\text{crystal}, s)$; the free energy of end pair defects at the center of the lamellae, ε ; the HPOSS NPs without close packing located at the surfaces (additional surface free energy due to entropic reasons), $\gamma_e(\text{NP}_s)$; and the squeezed HPOSS NPs at the surfaces (due to overcrowding), $\gamma_e(\text{NP}_H)$. With the help of the T_m of pure PEO($s = 1$) crystals (60.4 °C) and PEO($s = 2$) crystals (55.9 °C) having a molecular weight of 3.8k g/mol,^{2–5} we can identify each of these four parameters based on the experimentally observed T_m values and thus their effects on thermodynamic stabilities. For normal polymer lamellar crystals, their T_m and lamellar thickness, l , can be described by the Thomson–Gibbs equation^{18,37}

$$T_m = T_m^0 [1 - 2\gamma_e / (l\Delta h_f)] \quad (1)$$

where T_m^0 is the equilibrium melting temperature of the corresponding crystal with an infinite size, Δh_f is the equilibrium heat of fusion, and γ_e is crystal surface free energy. For the lamellar crystals having fold/end surfaces with the NPs, the γ_e term includes both contributions of the crystals, $\gamma_e(\text{crystal}, n)$, and NPs, $\gamma_e(\text{NP}) = \gamma_e(\text{NP}_s) + \gamma_e(\text{NP}_H)$. We know that the HPOSS NPs located at the surfaces are loosely and short-range-ordered packed in the PEO($s = 2.5$) and PEO($s = 2$) crystals, and thus, $\gamma_e(\text{NP}_H) = 0$. If NPs are squeezed and closely packed on the PEO($s = 1.5$) crystals' surface, $\gamma_e(\text{NP}_H) \neq 0$, while $\gamma_e(\text{NP}_s) = 0$. On the other hand, to account for the effect of the end pair defects located at the crystal center on T_m , the Sanchez–Eby equation approximately teaches^{38,39}

$$T_m = T_m^0 [1 - 2\gamma_e / (l\Delta h_f) - \varepsilon X / \Delta h_f] \quad (2)$$

where ε is the excess free energy of defects created by the incorporation of a mole of end pairs in the crystal lattice and X is the volume fraction of the defects in the crystals. X can be estimated if one considers that end pair defects are exactly located at the center of the crystals and affect their neighboring stems. The X value can be calculated by $X = N_{\text{defects}}/N$, where N_{defects} is the volume (repeat unit) occupied by the defects inside of each stem, which here can be estimated as 1.0, and N are the repeat units of each PEO stem [for PEO($s = 1.5$), $N = 57$, and for PEO($s = 2.5$), $N = 34$].

For the normal IF crystals in LMW PEOs, their average fold/end surface free energy $\gamma_e(\text{crystal}, s)$ can be calculated based on^{2–5}

$$\gamma_e(\text{crystal}, s) = \frac{[\gamma_{e,e}(\text{crystal}, s) + \gamma_{e,f}(\text{crystal}, s)]}{s} \quad (3)$$

where $\gamma_{e,e}(\text{crystal}, s)$ and $\gamma_{e,f}(\text{crystal}, s)$ represent the chain end and chain fold surface free energies of LMW PEO, respectively. Depending on the number of chain folds, $\gamma_{e,e}(\text{crystal}, s)$ is equal to 25.5 erg/cm² when $s = 1$ and 34.9 erg/cm² when $s \geq 2$. $\gamma_{e,f}(\text{crystal}, s)$ was found to be 22.4 erg/cm². The average fold/end surface free energy of a pure LMW PEO can thus be calculated based on eq 3 assuming that those half-stemmed crystals are also stabilized, and they are $\gamma_e(\text{crystal}, s = 1.5) =$

26.6 erg/cm², $\gamma_e(\text{crystal}, s = 2) = 28.7 \text{ erg/cm}^2$, and $\gamma_e(\text{crystal}, s = 2.5) = 24.9 \text{ erg/cm}^2$, respectively. Given that the T_m of the pure PEO($s = 2$) crystals with 3.8k g/mol is 55.9 °C and the T_m of PEO($s = 2$) for HPOSS-PEO_{3.8k} is 53.3 °C, we can deduce the effect of HPOSSs on the crystal surface without close packing, $\gamma_e(\text{NP}_s)$ using eq 1, because the pure PEO($s = 2$) crystal keeps its stability invariant during the study and thus is always at this local equilibrium. The overall $\gamma_e(s = 2)$ obtained is 31.0 erg/cm². The $\gamma_e(\text{NP}_s)$ at the crystal surface contributes to the overall $\gamma_e(s = 2)$ is thus 2.3 erg/cm² [$\gamma_e(s = 2) - \gamma_e(\text{crystal}, s = 2)$, 31.0–28.7 erg/cm²].

In order to obtain the value ε of end pairs within the PEO($s = 2.5$) crystals, we assume that the contribution of NPs is identical to that of the PEO($s = 2$) crystals (2.3 erg/cm²). The overall $\gamma_e(s = 2.5)$ is 27.2 erg/cm² (24.9 + 2.3 erg/cm²). Using eq 2, the ε value can thus be calculated to be 29.8 erg/cm². Furthermore, assuming that the ε value of PEO($s = 1.5$) crystals is identical to that deduced in the PEO($s = 2.5$) crystals (29.8 erg/cm²), we can calculate the overall $\gamma_e(s = 1.5)$ value based on eq 2, which is 34.8 erg/cm². In the first approximation, therefore, the overall $\gamma_e(\text{NP})$ is 8.2 erg/cm² (34.8 – 26.6 erg/cm²), which can be fully attributed to $\gamma_e(\text{NP}_H)$ because entropic contribution in this situation is negligible.

The final question is whether this observation is unique for the specific POSS-related GMSAs or it represents a general universality. We have designed a new GMSA molecule having [60]fullerene (C₆₀) NPs as a head and the same PEO as a tail, C₆₀-PEO_{3.8k}.^{40,41} Utilizing the same analysis, we can identify PEO($s = 2.5$) (black), PEO($s = 2$) (red), and PEO($s = 1.5$) (blue) crystals based on the relationship between L and T_x as shown in Figure 3 (compared to Figure 1a. For detailed

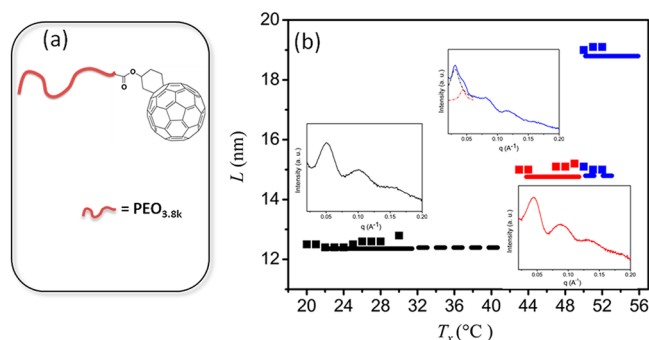


Figure 3. Schematic drawing of the molecular structure (a) and relationships between the L and T_x (b) for C₆₀-PEO_{3.8k}. Solid squares represent experimental data of the PEO($s = 2.5$) (black), PEO($s = 2$) (red), and PEO($s = 1.5$) (blue) crystals. Solid and dashed lines are the calculated values (see the SI).

analysis, see the SI). The only difference here is that for C₆₀-PEO_{3.8k}, no pure PEO($s = 1.5$) crystals can be isolated, but they always show a mixture with the PEO($s = 2$) crystals. This may be due to a larger cross-sectional area and geometrical incompatibility of C₆₀, compared to that of HPOSS,⁴² and lead to an average of more than three PEO stems to balance the cross-sectional areas between C₆₀ heads and PEO tails. Further analysis for this system is the focus of future work.

In summary, by properly designing molecules, new physical phenomena can be explored in the GMSA case having the HPOSS head with a PEO tail. The molecules build up double HPOSS layered structures in between the PEO lamellar crystals. In order to balance the cross-sectional areas between

the HPOSSs and the PEO crystal stem numbers, the IF and exactly defined half-stemmed crystals are observed (in this case, $s = 2.5$, 2, and 1.5). These findings may possess a general universality of the GMSAs with other types of NPs such as C₆₀. Note that without these NPs, these exactly defined half-stemmed crystals with precisely controlled defects at the center of the lamellar crystals are not stabilized and have not been observed because they prefer to be further organized into the IF crystals. However, after imposing the geometric restriction of NPs chemically connected to the PEO, the half-stemmed PEO crystals are now settled in free-energy minima and experimentally observable.

■ ASSOCIATED CONTENT

Supporting Information

The syntheses and detailed experimental procedures along with ¹H NMR spectra, SEC chromatography images, MALDI TOF spectra, and SAXS patterns of HPOSS-PEO_{3.8k} and BPOSS-PEO_{3.8k}. This material is available free of charge via the Internet at <http://pubs.acs.org>.

■ AUTHOR INFORMATION

Corresponding Author

*E-mail: wz8@uakron.edu (W.-B.Z.); scheng@uakron.edu (S.Z.D.C.). Phone: +1 330 972 6931. Fax: +1 330 972 8626.

Present Address

[†]R.V.H.: Department of Chemistry, Allegheny College, Meadville, PA 16335, U.S.A.

Notes

The authors declare no competing financial interest.

■ ACKNOWLEDGMENTS

This research was supported by the National Science Foundation (DMR-0906898, DMR-0821313, and CH2-1012636). We thank the Joint-Hope Education Foundation for generous research funding support.

■ REFERENCES

- (1) Arlie, P.; Spegt, P. A.; Skoulios, A. Etude de la Cristallisation des Polymères. I. Structure Lamellaire de Polyoxyéthylène de Faible Masse Moléculaire. *Markomol. Chem.* **1966**, *99*, 160–174.
- (2) Kovacs, A. J.; Gonthier, A. Crystallization and Fusion of Self-seeded Polymers. II. Growth Rate, Morphology, and Isothermal Thickening of Single Crystals of Low Molecular Weight Poly(ethylene oxide) Fractions. *Kolloid Z. Z. Polym.* **1972**, *250*, 530–551.
- (3) Kovacs, A. J.; Gonthier, A.; Straupe, C. Isothermal Growth, Thickening, and Melting of Poly(ethylene oxide) Single Crystals in The Bulk. *J. Polym. Sci., Polym. Symp.* **1975**, *50*, 283–325.
- (4) Kovacs, A. J.; Straupe, C.; Gonthier, A. Isothermal Growth, Thickening, and Melting of Poly(ethylene oxide) Single Crystals in The Bulk. II. *J. Polym. Sci., Polym. Symp.* **1977**, *59*, 31–54.
- (5) Kovacs, A. J.; Straupe, C. Isothermal Growth, Thickening, and Melting of Poly(ethylene oxide) Single Crystals in The Bulk. Part IV. Dependence of Pathological Crystal Habits on Temperature and Thermal History. *Faraday Discuss. Chem. Soc.* **1979**, *68*, 225–239.
- (6) Ungar, G.; Stejny, J.; Keller, A.; Bidd, I.; Whiting, M. C. The Crystallization of Ultralong Normal Paraffins: The Onset of Chain Folding. *Science* **1985**, *229*, 386–389.
- (7) Zeng, X.; Ungar, G.; Spells, S.; Brooke, G.; Farren, C.; Harden, A. Crystal–Amorphous Polymer Interface Studied by Neutron and X-ray Scattering on Labeled Binary Ultralong Alkanes. *Phys. Rev. Lett.* **2003**, *90*, 155508–1–4.
- (8) Zeng, X.; Ungar, G. Novel Layered Superstructures in Mixed Ultralong *n*-Alkanes. *Phys. Rev. Lett.* **2001**, *86*, 4875–4878.

- (9) Ungar, G.; Keller, A. Inversion of The Temperature Dependence of Crystallization Rates Due to Onset of Chain Folding. *Polymer* **1987**, *28*, 1899–1907.
- (10) Ungar, G.; Keller, A. Time-Resolved Synchrotron X-ray Study of Chain-Folded Crystallization of Long Paraffins. *Polymer* **1986**, *27*, 1835–1844.
- (11) Cheng, S. Z. D.; Wu, S. S.; Chen, J.; Zhuo, Q.; Quirk, R. P.; von Meerwall, E. D.; Hsiao, B. S.; Habenschuss, A.; Zsack, P. R. Isothermal Thickening and Thinning Processes in Low Molecular Weight Poly(ethylene oxide) Fractions Crystallized from the Melt. 4. End-Group Dependence. *Macromolecules* **1993**, *26*, 5105–5117.
- (12) Cheng, S. Z. D.; Zhang, A.; Chen, J.; Heberer, D. P. Nonintegral and Integral Folding Crystal Growth in Low-Molecular Mass Poly(ethylene oxide) Fractions. I. Isothermal Lamellar Thickening and Thinning. *J. Polym. Sci., Polym. Phys. Ed.* **1991**, *29*, 287–297.
- (13) Cheng, S. Z. D.; Zhang, A.; Barley, J. S.; Chen, J.; Habenschuss, A.; Zsack, P. R. Isothermal Thickening and Thinning Processes in Low Molecular Weight Poly(ethylene oxide) Fractions. I. From Non-integral-Folding to Integral-Folding Chain Crystal Transitions. *Macromolecules* **1991**, *24*, 3937–3944.
- (14) Cheng, S. Z. D.; Chen, J.; Barley, J. S.; Zhang, A.; Habenschuss, A.; Zsack, P. R. Isothermal Thickening and Thinning Processes in Low Molecular Weight Poly(ethylene oxide) Fractions Crystallized from the Melt. 3. Molecular Weight Dependence. *Macromolecules* **1992**, *25*, 1453–1460.
- (15) Chen, E.-Q.; Lee, S.-W.; Zhang, A.; Moon, B.-S.; Harris, I. M. W.; Cheng, S. Z. D. Isothermal Thickening and Thinning Processes in Low-Molecular-Weight Poly(ethylene oxide) Fractions Crystallized from the Melt. 8. Molecular Shape Dependence. *Macromolecules* **1999**, *32*, 4784–4793.
- (16) Ungar, G.; Zeng, X.-B. Learning Polymer Crystallization with the Aid of Linear, Branched and Cyclic Model Compounds. *Chem. Rev.* **2001**, *101*, 4157–4188.
- (17) Ungar, G.; Putra, E. G. R.; de Silva, D. S. M.; Shcherbina, M. A.; Waddon, A. J. The Effect of Self-Poisoning on Crystal Morphology and Growth Rates. *Adv. Polym. Sci.* **2005**, *180*, 45–87.
- (18) Cheng, S. Z. D. *Phase Transitions in Polymers The Role of Metastable States*; Elsevier: Amsterdam, The Netherlands, 2008.
- (19) Horsch, M.; Zhang, Z.; Glotzer, S. Self-Assembly of Polymer-Tethered Nanorods. *Phys. Rev. Lett.* **2005**, *95*, 056105/1–056105/4.
- (20) Glotzer, S. C.; Solomon, M. J. Anisotropy of Building Blocks and Their Assembly into Complex Structures. *Nat. Mater.* **2007**, *6*, 557–562.
- (21) Yu, X.; Yue, K.; Hsieh, I.-F.; Li, Y.; Dong, X.-H.; Liu, C.; Xin, Y.; Wang, H.-F.; Shi, A.-C.; Cheng, S. Z. D.; et al. Giant Surfactants Provide a Versatile Platform for Sub-10-nm Nanostructure Engineering. *Proc. Natl. Acad. Sci. U.S.A.* **2013**, *110*, 10078–10083.
- (22) Zhu, L.; Cheng, S. Z. D.; Calhoun, B. H.; Ge, Q.; Quirk, R. P.; Thomas, E. L.; Hsiao, B. S.; Yeh, F.; Lotz, B. Crystallization Temperature Dependent Crystal Orientations within Nanoscale Confined Lamellae of a Self-Assembled Crystalline–Amorphous Diblock Copolymer. *J. Am. Chem. Soc.* **2000**, *122*, 5957–5967.
- (23) Loo, Y.-L.; Register, R. A.; Ryan, A. J. Polymer Crystallization in 25-nm Spheres. *Phys. Rev. Lett.* **2000**, *84*, 4120–4123.
- (24) Huang, P.; Zhu, L.; Cheng, S. Z. D.; Ge, Q.; Quirk, R. P.; Thomas, E. L.; Lotz, B.; Hsiao, B. S.; Liu, L.; Yeh, F. Crystal Orientation Changes in Two-Dimensionally Confined Nanocylinders in a Poly(ethylene oxide)-*b*-polystyrene/Polystyrene Blend. *Macromolecules* **2001**, *34*, 6649–6657.
- (25) Zhu, L.; Huang, P.; Cheng, S.; Ge, Q.; Quirk, R.; Thomas, E.; Lotz, B.; Wittmann, J.-C.; Hsiao, B.; Yeh, F.; et al. Dislocation-Controlled Perforated Layer Phase in a PEO-*b*-PS Diblock Copolymer. *Phys. Rev. Lett.* **2001**, *86*, 6030–6033.
- (26) Loo, Y.-L.; Register, R. A.; Ryan, A. J.; Dee, G. T. Polymer Crystallization Confined in One, Two, or Three Dimensions. *Macromolecules* **2001**, *34*, 8968–8977.
- (27) Loo, Y.-L.; Register, R. A.; Ryan, A. J. Modes of Crystallization in Block Copolymer Microdomains: Breakout, Templated, and Confined. *Macromolecules* **2002**, *35*, 2365–2374.
- (28) Huang, P.; Zhu, L.; Guo, Y.; Ge, Q.; Jing, A. J.; Chen, W. Y.; Quirk, R. P.; Cheng, S. Z. D.; Thomas, E. L.; et al. Confinement Size Effect on Crystal Orientation Changes of Poly(ethylene oxide) Blocks in Poly(ethylene oxide)-*b*-polystyrene Diblock Copolymers. *Macromolecules* **2004**, *37*, 3689–3698.
- (29) Angelescu, D.; Harrison, C.; Trawick, M.; Register, R.; Chaikin, P. Two-Dimensional Melting Transition Observed in a Block Copolymer. *Phys. Rev. Lett.* **2005**, *95*, 025702/1–025702/4.
- (30) Lin, M. C.; Wang, Y. C.; Chen, H. L.; Muller, A. J.; Su, C. J.; Jeng, U. S. Critical Analysis of the Crystal Orientation Behavior in Polyethylene-Based Crystalline–Amorphous Diblock Copolymer. *J. Phys. Chem. B* **2011**, *115*, 2494–2502.
- (31) Lin, M. C.; Chen, H. L.; Lin, W. F.; Huang, P. S.; Tsai, J. C. Crystallization of Isotactic Polypropylene under the Spatial Confinement Templated by Block Copolymer Microdomains. *J. Phys. Chem. B* **2012**, *116*, 12357–12371.
- (32) Larsson, K. The Crystal Structure of Octa-(silsesquioxane). *Ark. Kemi* **1960**, *16*, 215–219.
- (33) Wurm, A.; Zhuravlev, E.; Eckstein, K.; Jehnichen, D.; Pospiech, D.; Androsch, R.; Wunderlich, B.; Schick, C. Crystallization and Homogeneous Nucleation Kinetics of Poly(ϵ -caprolactone) (PCL) with Different Molar Masses. *Macromolecules* **2012**, *45*, 3816–3828.
- (34) Chen, W.; Zheng, J.; Cheng, S.; Li, C.; Huang, P.; Zhu, L.; Xiong, H.; Ge, Q.; Guo, Y.; Quirk, R.; et al. Onset of Tethered Chain Overcrowding. *Phys. Rev. Lett.* **2004**, *93*, 028301/1–028301/4.
- (35) Zheng, J. X.; Xiong, H.; Chen, W. Y.; Lee, K.; Van Horn, R. M.; Quirk, R. P.; Lotz, B.; Thomas, E. L.; Shi, A.-C.; Cheng, S. Z. D. Onsets of Tethered Chain Overcrowding and Highly Stretched Brush Regime via Crystalline–Amorphous Diblock Copolymers. *Macromolecules* **2006**, *39*, 641–650.
- (36) Van Horn, R. M.; Zheng, J. X.; Sun, H.-J.; Hsiao, M.-S.; Zhang, W.-B.; Dong, X.-H.; Xu, J.; Thomas, E. L.; Lotz, B.; Cheng, S. Z. D. Solution Crystallization Behavior of Crystalline–Crystalline Diblock Copolymers of Poly(ethylene oxide)-*block*-poly(ϵ -caprolactone). *Macromolecules* **2010**, *43*, 6113–6119.
- (37) Cheng, S. Z. D. Materials Science: Polymer Crystals Downsized. *Nature* **2007**, *448*, 1006–1007.
- (38) Sanchez, I. C.; Eby, R. K. Thermodynamics and Crystallization of Random Copolymers. *Macromolecules* **1975**, *8*, 638–641.
- (39) Sanchez, I. C. Problems and Theories of Polymer Crystallization. *J. Polym. Sci., Polym. Symp.* **1977**, *59*, 109–120.
- (40) Zhang, W.-B.; Tu, Y.; Ranjan, R.; Van Horn, R. M.; Leng, S.; Wang, J.; Polce, M. J.; Wesdemiotis, C.; Quirk, R. P.; Newkome, G. R.; et al. “Clicking” Fullerene with Polymers: Synthesis of [60]Fullerene End-Capped Polystyrene. *Macromolecules* **2008**, *41*, 515–517.
- (41) Dong, X.-H.; Zhang, W.-B.; Li, Y.; Huang, M.; Zhang, S.; Quirk, R. P.; Cheng, S. Z. D. Synthesis of Fullerene-Containing Poly(ethylene oxide)-*block*-polystyrene as Model Shape Amphiphiles with Variable Composition, Diverse Architecture, and High Fullerene Functionality. *Polym. Chem.* **2012**, *3*, 124–134.
- (42) Hirsch, A.; Brettreich, M. *Fullerenes: Chemistry and Reactions*; Wiley-VCH: Weinheim, Germany, 2005.